



# Weak protein–protein interactions in live cells are quantified by cell-volume modulation

Shahar Sukenik<sup>a</sup>, Pin Ren<sup>b</sup>, and Martin Gruebele<sup>a,b,c,1</sup>

<sup>a</sup>Department of Chemistry, University of Illinois at Urbana–Champaign, Urbana, IL 61801; <sup>b</sup>Department of Physics, University of Illinois at Urbana–Champaign, Urbana, IL 61801; and <sup>c</sup>Center for Biophysics and Computational Biology, University of Illinois at Urbana–Champaign, Urbana, IL 61801

Edited by Angela M. Gronenborn, University of Pittsburgh School of Medicine, Pittsburgh, PA, and approved May 18, 2017 (received for review January 16, 2017)

**Weakly bound protein complexes play a crucial role in metabolic, regulatory, and signaling pathways, due in part to the high tunability of their bound and unbound populations. This tunability makes weak binding (micromolar to millimolar dissociation constants) difficult to quantify under biologically relevant conditions. Here, we use rapid perturbation of cell volume to modulate the concentration of weakly bound protein complexes, allowing us to detect their dissociation constant and stoichiometry directly inside the cell. We control cell volume by modulating media osmotic pressure and observe the resulting complex association and dissociation by FRET microscopy. We quantitatively examine the interaction between GAPDH and PGK, two sequential enzymes in the glycolysis catalytic cycle. GAPDH and PGK have been shown to interact weakly, but the interaction has not been quantified in vivo. A quantitative model fits our experimental results with  $\log K_d = -9.7 \pm 0.3$  and a 2:1 prevalent stoichiometry of the GAPDH:PGK complex. Cellular volume perturbation is a widely applicable tool to detect transient protein interactions and other biomolecular interactions in situ. Our results also suggest that cells could use volume change (e.g., as occurs upon entry to mitosis) to regulate function by altering biomolecular complex concentrations.**

quinary interactions | protein–protein interactions | cell volume | FRET | live-cell microscopy

**F**rom forming active enzymatic complexes to facilitating signal transduction in regulatory networks, protein interactions are pivotal to cell function. Strong interactions, with dissociation constants ( $K_d$ ) of nanomolar and lower (1, 2), can be measured accurately both in vitro and in vivo (3, 4). These interactions are ideal in cases where the complex should form with high fidelity and persist. The downside of strong binding is that its regulation in the cellular environment is limited: Once a complex is formed, it seldom dissociates.

Another type of protein complexes relies on weak, transient interactions, collectively termed quinary interactions (5–7). Such interactions, with a  $K_d$  in the micromolar to millimolar range, are emerging as important components of the cell's signaling, regulatory, and stress adaptation mechanisms (6, 8, 9). Their transient nature is key to their function: Unlike tightly bound complexes, quinary interactions are highly sensitive to variations in their environment and respond rapidly to changes in temperature, pressure, pH, or the local concentration of surrounding molecules. The sensitivity of quinary interactions makes them important in fine-tuning cellular processes. For example, it has been proposed that sequential metabolic enzymes could associate to improve substrate transfer between catalytic enzymes (10), that weak protein association can mediate cytokine release (11), or that phase-separated protein droplets held together by quinary interactions could serve for cellular storage or stress response (12, 13).

Despite growing interest, quantification of quinary interactions is technically challenging because it requires detection in situ using a mildly perturbing technique (6, 14). Previous studies of quinary interactions rely on measurements of large cell populations expressing labeled proteins, e.g., through the use of in-

cell NMR with *Escherichia coli* (15, 16). Others rely on observations of large macromolecular aggregates that are visible as foci under a microscope and lack a fixed stoichiometry, in a process more akin to phase separation (9, 17, 18).

We show that a perturbation to cell volume can detect and measure quinary interactions. Volume change is a mild perturbation that happens routinely: Cells change their volume by up to 30% in both routine cell-cycle changes and in response to deleterious conditions (19–21). Rapid volume changes (approximately 1–100 s) are driven by water influx or efflux, altering the concentration of all molecular species contained within the cellular matrix (19, 22, 23). At such short times, regulatory actions taken by the cell to cope with the change in volume, such as synthesizing channels, chaperones, and enzymes are scarcely initiated (24, 25). Thus, fast volume change affects viscosity (26), crowding (27, 28), protein structure (29, 30), activity (31), and quinary interactions within the cell purely by physico-chemical means. Cell volume can be controlled by changing medium osmotic pressure—another parameter that varies in biological settings: Extracellular osmolarity fluctuates routinely for some mammalian cells, including kidney (32), cartilage (33), and even in the blood under certain pathological conditions (34).

We subject adhered mammalian cells (U-2 OS) to osmotic stress, increasing or decreasing their volume. A sudden change of cell volume causes the population of protein(s) of interest to reequilibrate between monomers and complex. By tagging the associating proteins of interest with fluorescent protein labels (FPs), we can observe this reequilibration process, and quantitatively determine  $K_d$  and the stoichiometry of the complex inside living cells. We first show that changes to cellular crowding conditions occur concomitantly with volume changes by using the synthetic crowding sensor fCrH2. Next, we examine two pairs of FPs, AcGFP1/mCherry and mEGFP/mCherry. The former pair interacts in cells to form heterooligomers, whereas the latter

## Significance

**Weak, transient protein complexes are emerging as vital to cell function and regulation, with roles ranging from stabilization of a protein structure to driving cytoplasmic phase separations. Because of their fleeting nature and sensitivity, such complexes are notoriously hard to characterize. We develop and validate a method to quantify such “quinary interactions” inside the cell itself, and apply it to the putative interaction of the glycolytic enzymes GAPDH and PGK. Our method can characterize weak protein–protein interactions in live cells, with future application to other biomolecular species, such as RNAs.**

Author contributions: S.S. and M.G. designed research; S.S. and P.R. performed research; S.S. and M.G. analyzed data; and S.S. and M.G. wrote the paper.

The authors declare no conflict of interest.

This article is a PNAS Direct Submission.

<sup>1</sup>To whom correspondence should be addressed. Email: mgruebel@illinois.edu.

This article contains supporting information online at [www.pnas.org/lookup/suppl/doi:10.1073/pnas.1700818114/-DCSupplemental](http://www.pnas.org/lookup/suppl/doi:10.1073/pnas.1700818114/-DCSupplemental).

does not, highlighting the importance of selecting proper FRET labels for quantitative in-cell studies of quinary interactions. Finally, we study the association of GAPDH and PGK in the context of the cell's cytoplasm—these two crucial glycolytic-cycle enzymes are thought to form transient complexes to expedite substrate turnover. We develop a quantitative model that relates changes in FRET to changes in equilibrium concentrations of free and complexed proteins. The model reproduces all experimental observables, extracting both the stoichiometry and  $K_d$  of complex formation within the cell.

Beyond quantifying weak protein interactions in situ, our results suggest that interaction networks (in our example, a small part of a metabolic network) can be altered by cellular volume change. Our model predicts that this sensitivity is particularly high when the dissociation constant  $K_d$  is of the order of the protein's cellular concentration. It is known that the cell changes its volume as part of an internal regulatory process, or in response to environmental duress (20, 23). We propose that such cellular volume change can trigger regulatory responses rapidly and reversibly, purely by altering the concentrations of complexed proteins, an effect that is amplified because the free volume (the volume that is occupied by water and other small, permeable solutes) in the cell is less than the overall cellular volume.

## Results

**Osmotic Modulation Approach.** Our setup interfaces an epifluorescence microscope with a temperature-controlled flow cell coupled to a pressure controller unit. Cell media normally has an osmolarity of  $\sim 0.3$  Osm. Deviations from this value induce cellular volume change across many different cell types (35). Our setup modulates the osmolarity of media flowing over the cells from isosmotic to either hypoosmotic or hyperosmotic conditions and back within seconds (*Methods*). Regulatory expression of proteins in response to the volume change is minimal at these times (24, 25). However, protein folding and protein-protein interactions, which often occur in seconds or less (36), readily respond to induced volume changes at these timescales (9).

Because cells can vary widely in shape, size, and cytoskeletal structure, we use the relative cell volume  $\tilde{v} = V/V_0$  as our adjustable parameter, where  $V_0$  is the isosmotic volume.  $\tilde{v}$  is expected to depend only on the amplitude of the osmotic challenge. To test this idea, we use confocal microscopy to examine the change in  $\tilde{v}$  following rapid osmolarity changes (Fig. 1A). Because water primarily drives volume change, whereas macromolecular content remains constant, we account for the relative free volume change,  $\tilde{v}_f = \tilde{v} - \tilde{v}_{occ}$ . The occupied relative volume  $\tilde{v}_{occ}$  in the cell, composed of all solutes that do not readily diffuse upon volume change, is estimated to be  $\sim 30\%$  in isosmotic conditions (37, 38). In Fig. 1B and *SI Appendix, Fig. S1*,  $\tilde{v}$  (and  $\tilde{v}_f$ ) is shown to be robust for the range of osmotic pressures tested.

We probe the response of proteins to changes in cell volume by observing the changes to donor (green) and acceptor (red) fluorescence emission using a FRET illumination setup (Fig. 1C). An experiment normally consists of observing the FRET fluorescence from a single cell while inducing cell-volume change. The green and red fluorescence intensity depends on the proximity and relative orientation of the donor and acceptor molecules (39). FRET pairs in close proximity and proper orientation will show a decrease in green and increase in red fluorescence compared with ones that are farther apart.

Cells display a change in green and red fluorescence during osmotic modulation only when the labeled proteins change structure or form complexes. The labels themselves show little or no response to volume changes when expressed separately (*SI Appendix, Fig. S2*). We use U-2 OS cells that cope well with the short duration of stress they are subjected to in this setup: There is rarely any blebbing or breakdown of the nuclear envelope. During duress, endosomal motility is arrested as reported (40), but recovers rapidly upon return to isosmotic conditions, even after the most extreme osmotic challenges (0.1 or 0.8 Osm; *Movie S1*).

We use media diluted with MilliQ water to induce volume increase, or supplemented with NaCl to induce decrease. To ensure that the volume effects are independent of the osmotic agent used,

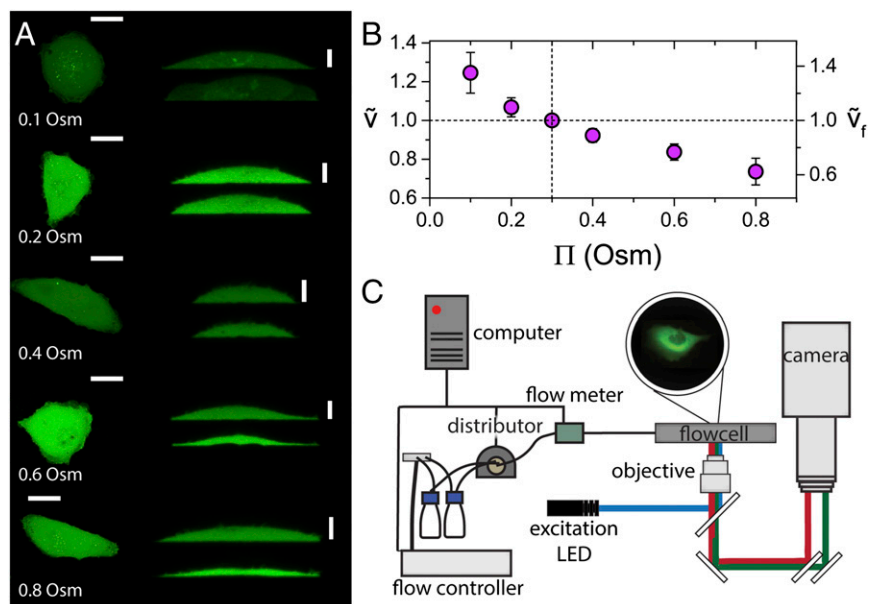


**Fig. 1.** Volume changes in response to osmotic pressure modulations. (A) Representative 3D confocal images of cells subjected to volume modulation. Image at *Left* shows maximum  $xy$  projection. Images at *Right* show an  $xz$  slice before (*Upper*) and 1 min after (*Lower*) osmotic challenge. (Scale bars:  $xy$ , 20  $\mu\text{m}$ ;  $xz$ , 10  $\mu\text{m}$ .) Changes in intensity before and after osmotic challenge are due to concentration changes of the loaded dye (calcein AM) resulting from volume modulation. (B) Average relative cell-volume change (compared with isosmotic conditions) as function of osmolarity (see *SI Appendix, Fig. S1* for details). Error bars are SD of the data from  $n > 10$  measurements of individual cells. (C) Volume-modulation experimental setup.

we also switched NaCl for equi-osmotic solutions of mannitol or glucose, both noncharged osmolytes. All cosolutes gave a similar change in green and red fluorescence in the most extreme volume change tested. (*SI Appendix, Fig. S3*).

**Crowding Tracks Cell-Volume Modulation.** To detect the correlation between cell-volume change and crowding in the cell, we use the crowding sensor CrH2 developed by Boersma et al. (28). Our fCrH2 construct uses AcGFP1 and mCherry as the FRET pair. We first studied fCrH2 in vitro by recombinantly expressing and purifying it. The relative change to in vitro FRET efficiency, defined in Eqs. 1 and 2, increases as the concentration of ficoll (a polymeric crowder) increases (Fig. 2A, details in *SI Appendix, section S2*). The protein displayed no sharp transition behavior, implying that fCrH2 undergoes a continuous structural change, as reported (28).

To demonstrate that fCrH2 FRET signal responds linearly to volume modulation inside cells, fCrH2 was transfected into adhered U-2 OS cells. After the onset of osmotic stress, the green and red channels change reciprocally (Fig. 2B and C), a hallmark

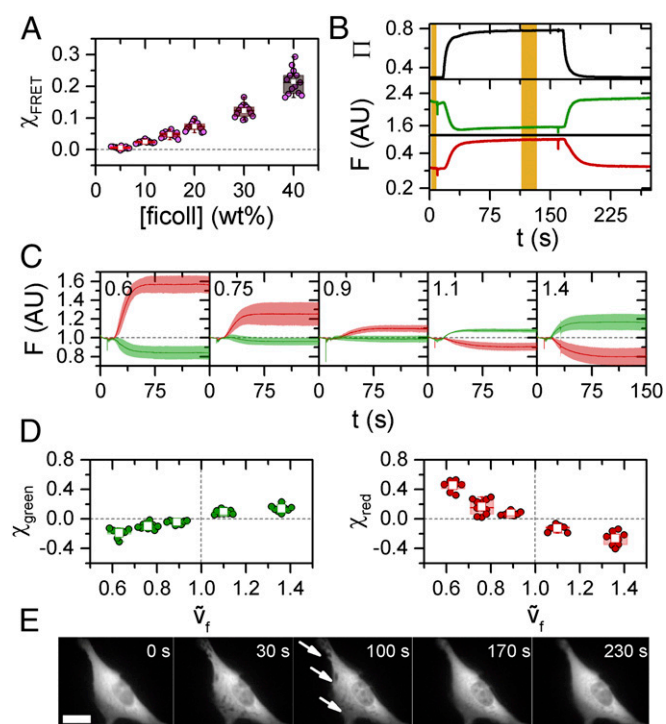


**Fig. 2.** Structural changes in fCrH2 in response to volume modulations. (A) Box chart showing relative FRET change of purified fCrH2 in increasing ficoll (polymeric crowder) concentrations.  $\chi_{\text{FRET}}$  is measured relative to the absence of ficoll. For all box charts in this work, boxes span from 25 to 75% of the data, with the median shown as a line, and SD shown as whiskers. Colored circles are data points from individual experiments, with the average shown as a white square. (B) Osmolarity in Osm (Upper), and cell-average green and red fluorescence (Lower) collected from a cell expressing fCrH2 and subjected to an osmotic shift to 0.8 Osm. The yellow regions are averaged and used to calculate  $\chi$  (Eq. 2). (C) Time traces of the normalized fluorescence changes to green and red fluorescence.  $\bar{v}_f$  is specified on the top left corner of each trace. Shaded areas are SD of the mean, which is shown as a line.  $n > 10$  for all data shown. (D) Relative changes to green (Left) and red (Right) fluorescence from data in C. The changes are shown as function of the relative free volume change,  $\bar{v}_f$ . (E) Snapshots of the same cell as B at different stages of the experiment. Upon shifts to 0.8 Osm, or upon return to isosmotic conditions from 0.1 Osm, cells exhibited invaginations in their membranes (arrows) that disappeared when iso-osmotic conditions were restored, as observed previously (59). (Scale bar: 10  $\mu\text{m}$ .)

of FRET. Once plateaued, the signal remains nearly constant, indicating that the crowding has reached a steady state. The plateauing of the fluorescence signal also means that no regulatory volume changes take place for the short duration of the experiments (19). Once the flow is switched back to isosmotic conditions, the fluorescence returns to basal levels, even after repeated volume change cycles (*SI Appendix, Fig. S4*). The reversibility of the fluorescence signal demonstrates the high resilience of the cells to volume changes and supports our assumption that it is primarily water that leaves or enters the cell. Data are represented as relative signal change,  $\chi$  (as described in Eq. 2, *Methods*) for green and red fluorescence, and shown for all volume changes in Fig. 2D. The magnitude of change in both green and red fluorescence correlated nearly linearly with the change in relative free volume. Throughout the entire experiment, cells retained their surface area as shown for a representative cell in Fig. 2E.

Our observations can be explained by molecular crowding theory (27, 41). When free volume decreases, fCrH2 responds by assuming a more compact conformation. For this protein, a more compact conformation brings the FPs at the termini closer, increasing FRET efficiency (more red, less green). The exact opposite happens during a volume increase. Indeed, a tethered control construct of AcGFP1-mCherry separated by 4 amino acids did not show a similar change in green and red fluorescence under the same perturbation (*SI Appendix, Fig. S5*). In addition, we observe that the protein responds rapidly to changes in cell volume, as revealed by the way the red and green fluorescence changes closely trace the osmolarity (Fig. 2B and *SI Appendix, Fig. S6*).

**Heterooligomerization of FPs Can Be Detected by Cell-Volume Modulation.** Moving on to putative quinary interactions, we first examine the association of commonly used FP labels. Wild-type FPs form homo-oligomers (42, 43) and have a high degree of sequence and structural homology, making heterooligomerization, even of engineered FPs, a realistic possibility. Fluorescent protein heterooligomerization presents problems in the interpretation of FRET and colocalization experiments, yet has scarcely been studied (44). In our experiment, FP heterooligomerization would mask the detection of protein-protein interactions.

We examined the AcGFP1/mCherry FRET pair by fluorescence titration in vitro and found that it associates with a  $K_d \sim 20 \mu\text{M}$  in PBS buffer at room temperature (Fig. 3A and *SI Appendix, Fig. S7*). To see whether association also occurs in vivo, we cotransfected these two FPs in U-2 OS cells with equal plasmid concentrations and used volume modulation to detect complex association and dissociation. For cotransfected cells, FRET signals are prone to artifacts arising from imbalanced expression levels (45). To circumvent artefactual fluorescence changes caused by imbalanced expression, we calibrated fluorescence intensities of purified FPs in vitro and used this calibration to select cells with similar expression levels of the two fluorescent proteins (*SI Appendix, Fig. S8*).

We find that AcGFP1 and mCherry associate in cells as well. Fig. 3B shows the reciprocal green and red fluorescence changes whose amplitude scales with  $\bar{v}_f$ . Importantly, the overall changes in  $\chi$  slope and amplitude are significantly different from the ones obtained with fCrH2 (Fig. 2C). To produce a comparable FRET signal in the absence of binding (i.e., from random proximity between nonassociated molecules), one would need concentrations of  $\sim 1 \text{ mM}$ , far higher than our few micromolar in-cell concentrations (39). Our quantitative analysis of in-cell  $K_d$  and association stoichiometry is described further below.

Next, we tested the mEGFP/mCherry pair. mEGFP contains the monomer-stabilizing mutation A206K. This pair showed a markedly diminished  $E_{\text{FRET}}$  (Eq. 1 in *Methods*) compared with AcGFP1 and mCherry (Fig. 3C). The change in green fluorescence

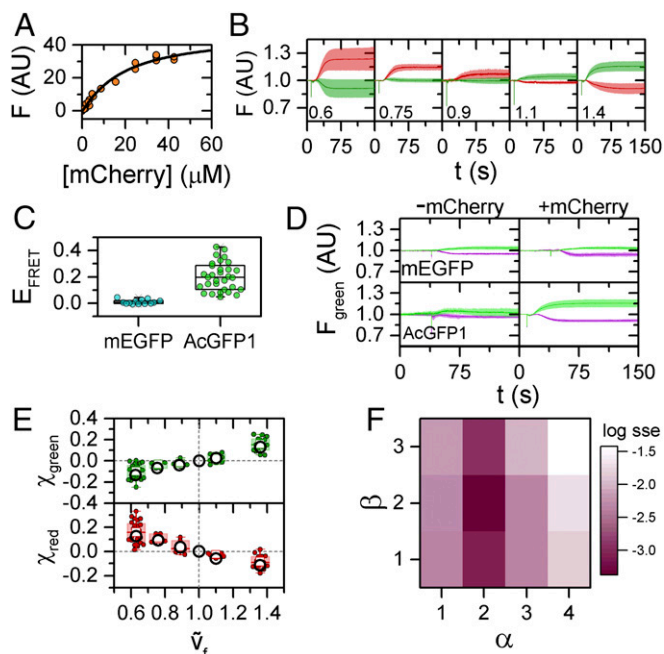


**Fig. 3.** Fluorescent protein association detected by volume modulations. (A) *In vitro* binding experiment shows AcGFP/mCherry association. Solid line is a concatenated fit of three experiments to the Hill equation, with  $K_d = 20 \pm 5 \mu\text{M}$ ,  $n = 1.1 \pm 0.1$  (see also *SI Appendix, Fig. S7*). (B) Changes to green and red fluorescence of cells coexpressing AcGFP1 and mCherry following volume modulation. Inset numbers are  $\bar{v}_t$ . Lines are averages of  $n > 10$  experiments for each volume modulation. Shaded areas are SD of the data. (C)  $E_{\text{FRET}}$  (Eq. 2, *Methods*) under isosmotic conditions is negligible for mEGFP in the presence of mCherry compared with AcGFP1. The high variability for AcGFP1 is a result of different expression levels in each cell. Box charts as in Fig. 2. (D) Time trace of changes to green fluorescence under volume increase (green, 0.1 Osm) and decrease (magenta, 0.8 Osm) perturbation shows a response only for AcGFP1, not mEGFP. Shaded areas represent SD of all repeats,  $n > 5$  for all experiments. (E)  $\chi$  values for green and red fluorescence for AcGFP1-mCherry, obtained from experiments shown in B. Box charts as in Fig. 2. Open circles are fits of the model to the experimental data (see *SI Appendix, Table S2* for fit constants). (F) Heat map showing log of the sum of square errors between fit and experimental results (sse) for different stoichiometries of AcGFP1 and mCherry ( $\alpha$  and  $\beta$ , respectively; see *SI Appendix, section S3* for details).

of mEGFP upon cellular volume change was identical in the presence and absence of mCherry, whereas AcGFP1 showed significant changes in green fluorescence under the same conditions (Fig. 3D). These data show that mEGFP does not interact with mCherry in cells, making the pair viable as FP labels for association studies of other proteins of interest.

**Quinary Interaction Between Two Metabolic Enzymes.** We applied the osmotic modulation technique to detect and measure the quinary interaction of two metabolic enzymes. It has been proposed that sequential metabolic enzymes, where the product of one is the substrate of the other, have evolved to weakly associate. Such association can dramatically improve substrate processing by reducing diffusion times between enzymes (10). Our targets, glyceraldehyde 3-phosphate dehydrogenase (GAPDH) and phosphoglycerate kinase (PGK), are one such pair. GAPDH and PGK catalyze the sixth and seventh steps in the glycolysis cycle, respectively. The GAPDH crystal structure is tetrameric (46), and has been shown to exist as the tetramer  $\text{GAPDH}_4$  under crowded conditions (47). PGK is known to exist as a monomer in the cytoplasm and has been extensively studied by us and others (31, 48, 49). These proteins have been shown to interact *in vitro* by using gel and affinity chromatography (50,

51). FRET fluorescence lifetime imaging of live cells was previously used to show that interaction occurs *in vivo* as well (52), but this method was unable to quantify the binding affinity or give insight into the stoichiometry of binding.

GAPDH was labeled with mEGFP close to the N-terminal and away from its tetramerization interface; PGK was labeled with mCherry at the N-terminal (see *SI Appendix, Table S1* for sequences). We coexpressed the two labeled proteins in U-2 OS cells, selected cells with similar concentrations of the two proteins for imaging, and applied our method to see how the FRET signal is affected by induced cellular volume change. The two metabolic enzymes associate in the cytoplasm of U-2 OS cells. Fig. 4A shows the reciprocal change in green and red fluorescence that signals GAPDH<sub>4</sub>/PGK interaction. We discuss the quantitative determination of  $K_d$  and association stoichiometry for GAPDH<sub>4</sub>/PGK and for the differently behaved AcGFP1/mCherry pair next.

**Analysis of Quinary Interactions Using a Quantitative Volume Modulation Model.** To quantify our experimental results, we developed a model that predicts the effect of volume change on the association equilibrium of our labeled proteins. The model relates the changes in two-color fluorescence seen upon volume modulation to reequilibration of the free and bound forms of the labeled proteins. Translating concentrations into fluorescence signal allows direct comparison with experimental observables. We have used this model to develop a rigorous fitting procedure for our experimental results, as shown in *SI Appendix, Fig. S10A*. A detailed description of the model, fitting procedures, constants used for fitting, error estimation, and a link to obtain the code can be found in *SI Appendix, section S3*.

Briefly, our fitting procedure considers a range of stoichiometries  $\alpha A + \beta B \rightleftharpoons A_\alpha B_\beta$  for the experimental data shown in Figs. 3E and 4B.  $\alpha$  and  $\beta$  are the stoichiometries,  $A$  and  $B$  are the molecules labeled with the donor and acceptor FPs, and  $A_\alpha B_\beta$  is the main complex responsible for the FRET signal. Our model starts with equilibrium concentrations of  $A$ ,  $B$ , and  $A_\alpha B_\beta$ , which

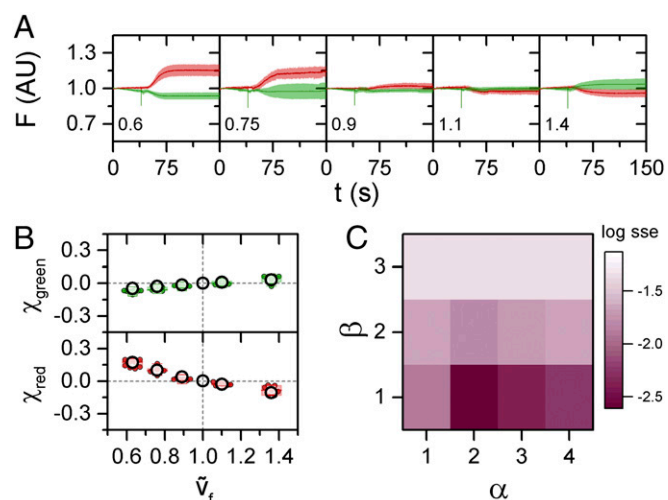


**Fig. 4.** GAPDH-PGK binding detected by volume modulations. (A) Changes to green and red fluorescence of cells coexpressing labeled GAPDH and PGK from volume modulations. Inset numbers are the osmolarity of the modulation. Lines are averages of  $n > 7$  experiments for each volume modulation. Shaded areas are SD of the data. (B)  $\chi$  values for green and red fluorescence for GAPDH-PGK. Box charts are as in Fig. 2. Open circles are fits of the model to the experimental data (see *SI Appendix, Table S2* for fit constants). (C) Heat map showing log of the sum of square errors between fit and experimental results (sse) for different stoichiometries of GAPDH and PGK ( $\alpha$  and  $\beta$ , respectively; see *SI Appendix, section S3* for details).

then change upon an osmotically induced volume change. The final concentrations are obtained by solving the differential rate equations for each species until a new equilibrium is reached. Multiple intermediate complexes can also be populated (and modeled by additional differential equations); for simplicity, we consider only the most probable association equilibrium, which fits our experiments well. For proteins with a concentration range between 1 and 15  $\mu\text{M}$ , our model predicts that significant changes to  $\chi$  will only occur in systems where  $K_d$  is in the 0.1–100  $\mu\text{M}$  range (*SI Appendix*, Fig. S10 B and C). The reaction order and  $K_d$  can be estimated from  $\chi_{\text{green}}$  and  $\chi_{\text{red}}$  as a function of cell-volume change (as shown in *SI Appendix*, section S3). Thus, our method is particularly useful for detection of weak quinary interactions between proteins inside cells (5, 14).

For the association between AcGFP1 and mCherry (Fig. 3E), the best fit is obtained with a  $2A + 2B \rightleftharpoons A_2B_2$  stoichiometry, as shown in Fig. 3F. The fitted  $\log K_d = -17.1 \pm 0.3$ , which corresponds to a dimerization  $K_d = 2.0 \pm 0.5 \mu\text{M}$ . The in-cell  $K_d$ , smaller by an order of magnitude from our *in vitro* experiment, ( $K_d \sim 20 \mu\text{M}$ ; Fig. 3A) indicates that the cellular matrix, either by crowding or quinary interactions, promotes association of this FP pair relative to the test tube (7). Additionally, the low cooperativity shown in our *in vitro* binding curve (Hill coefficient of  $\sim 1$ , Fig. 3A) does not agree with the higher association order found *in vivo*. The discrepancy indicates that the cellular environment not only modulates binding affinity, but can also affect the binding mechanism and promote the formation of higher order complexes (6). The heat map of the fit quality vs. stoichiometric coefficients in Fig. 3F shows that  $\alpha = 2$  (AcGFP1) is strongly favored, but that other values of  $\beta$  (mCherry) may also be populated. Indeed, AcGFP1 is known to form dimers, whereas mCherry is strictly monomeric. Thus, complex size is not likely to be completely homogeneous in terms of the number of mCherry molecules involved.

Fig. 4B shows  $\chi$  for green and red fluorescence of GAPDH/PGK complexation. Fitting our model to these experimental results shows that an overall equilibrium of  $2A + B \rightleftharpoons A_2B$ , where  $A$  is GAPDH tetramer (53) and  $B$  is PGK, gives the best fit to the data (Fig. 4C). We obtain  $\log K_d = -9.7 \pm 0.3$ , equivalent to a dimerization  $K_d$  of  $14 \pm 6 \mu\text{M}$  at cellular protein concentrations. Our model predicts a prevalent 2:1 stoichiometry of GAPDH<sub>4</sub> with PGK. We assume the GAPDH is in tetrameric form because the dissociation constant for  $4\text{GAPDH} \rightleftharpoons \text{GAPDH}_4$  in crowded conditions was found to be  $\log K_d \sim -25$  (47), implying tight binding that should not be perturbed by volume modulation. Thus, we propose that at least two GAPDH<sub>4</sub> tetramers associate with a single PGK molecule in to a weakly bound quinary complex. In line with our results, the turnover rate of wild-type PGK is known to be higher than GAPDH [ $\sim 200 \text{ s}^{-1}$  for GAPDH tetramers (54) vs.  $\sim 800 \text{ s}^{-1}$  for PGK monomers (55)], and PGK copy numbers are known to be at least a factor of 2 smaller than GAPDH levels in U-2 OS cells (56). We also considered the possibility of tetramers that contain a mix of labeled and unlabeled GAPDH, due to the high concentrations of GAPDH that exist in U-2 OS cells (56). Our model shows little sensitivity to a mix of fluorescent and nonfluorescent proteins in the tetramer, as discussed in *SI Appendix*, section S3 and Fig. S15.

## Discussion

Our results show that free volume modulation can be exploited to reveal the binding affinity and stoichiometry of weakly bound complexes inside the cell. Osmotically induced volume changes are reversible and can be explained in terms of a return to new steady-state concentrations of complexes following the volume change. We could determine the preferred association stoichiometry for GAPDH<sub>4</sub>/PGK as well as the binding strength. A caveat from our FP control experiments is that not every FP-label pair is suitable for determining quinary association, because some pairs may interact by themselves and mask association of proteins of interest.

Rapid volume changes will alter the concentrations of all species in the cell, affecting ionic strength, pH, and concentration of other molecules. Our model fits the full set of volume data, including near  $V = V_0$  ( $\tilde{v} = 1$ ) where the perturbation vanishes, thus representing the unperturbed  $K_d$  and stoichiometry inside cells. Volume changes up to 30% did not significantly affect the binding constants or thermodynamics, as indicated by the good fits of the model (Figs. 3E and 4B). It is possible that some associating protein pairs will have a  $K_d$  or stoichiometry that depends on other variables affected by the volume, e.g., ionic strength for a highly charged protein pair. In such cases, modulation of volume should not deviate too far from the iso-osmotic condition of  $\sim 0.3$  Osm to measure association under native conditions.

An interesting hypothesis raised by our results is that the cell environment is finely tuned to optimize weak interactions networks among its protein machinery (in our example, metabolic proteins). Such weak interaction networks create the possibility of a “fuzzy” interaction network in the cell (57), in contrast to the binary on-off nature of tight binding networks. In fact, the sensitivity of weak complex populations to cellular volume changes suggests a class of protein complexes whose association strongly depends on cellular crowding conditions. Such complexes imbue the cell with the ability to detect, signal, and/or directly initiate regulatory processes quickly and effectively in response to external stresses or internal signals, such as the rapid volume increase that occurs upon entry to mitosis (20, 23).

Some studies of in-cell interactions (13, 17) have observed microscopic phase changes in the cytoplasm. Our microscopy data does not show the appearance of foci upon volume change, and our predicted stoichiometry peaks at low numbers, rather than the limit  $\alpha, \beta \rightarrow \infty$ . Thus, our approach is complementary to imaging phase changes (58) inside cells. It would be interesting to see whether oligomerization can be detected by our method before foci appear, revealing early stages of such phase changes, in analogy to oligomers vs. fibrils for amyloids.

## Methods

**Osmotic Modulation FRET Microscopy.** U-2 OS cells (ATCC) grown in DMEM (Corning) supplemented with 10% FBS (Sigma) and 5% penicillin streptomycin (Sigma) were transfected with the appropriate plasmid(s) with Lipofectamine 2000 (Thermo-Fisher) using standard protocol, and plated after 5–6 h of incubation on a treated 40-mm round 1.5 coverslip. Before imaging, the coverslip was washed twice with PBS, covered with FluoroBrite medium (Thermo-Fisher), and placed in a flow cell with a 200- $\mu\text{m}$ -thick rectangular gasket (FCS2, Biopetech). Cells were imaged between 18 and 22 h after transfection. The flow controller (ElveFlow), controlled using home-built software written with LabView (National Instruments), was used to flow medium at 3 mL/min through the flow cell. This flowrate was selected as an optimal value that gives fast medium switches, with little flow-related focus drifts. Hypoosmotic media was prepared by dilution of media with MilliQ water, and hyperosmotic media by addition of an appropriate amount of NaCl. Medium osmolarity was verified by using vapor-pressure osmometry with a Wescor Vapro 5520 osmometer. A standard profile flowed 40 s of iso-osmotic media before switching to a nonisosmotic media for 150 s, and then switching back to isosmotic media for another 40 s.

The flow rate must be held constant during imaging because fluctuations of the flow rate larger than  $\sim 5\%$  create a focus shift that interferes with fluorescence intensity readings. To circumvent this problem, the pressure controller is coupled to a flow sensor placed upstream of the flow cell. Using a PID algorithm, the flow is controlled to  $\sim 3\%$  accuracy (*SI Appendix*, Fig. S9A), allowing for seamless imaging with minimal interference during flow switching. Media osmolarity is quantified by following a fluorescent dye added to the nonisosmotic media (*SI Appendix*, Fig. S9B).

The volume change induced by an osmotic challenge occurs within seconds (in our setup, the volume change is often limited by the osmolarity gradient caused by medium switching; *SI Appendix*, Fig. S6), and although the binding/unbinding kinetics of some slow-associating proteins may become rate-determining, this did not occur for the proteins we investigated here.

Proteins were tagged with either GFP (donor) or mCherry (acceptor), or both for fCrH2. A 470-nm mounted LED (ThorLabs, M470-L3) was used to

excite the donor, and a 590 nm LED (ThorLabs, M590-L3) was used for direct excitation of the acceptor. The emitted light was split by using a downstream dichroic optic (Chroma), and the separated channels were projected as separate spots on a phantom V12.1 CMOS camera imaging at 24 frames per s. FRET efficiency was calculated by using bleach corrected data (see *SI Appendix, section S2*), with the ratio

$$E_{\text{FRET}} = \frac{F_{\text{red}}}{F_{\text{red}} + F_{\text{green}}} \quad [1]$$

Here,  $F_{\text{green}}$  and  $F_{\text{red}}$  are the fluorescence intensities in the green and red channels. Notably, cell average FRET signal was insensitive to the method of calculation: Obtaining cell-wide averages for each channel and dividing those gave nearly identical values to the average of the ratio between single pixels in each channel. Because signals vary from cell to cell depending on expression levels and cell shape, the relative change  $\chi$  of signal  $S$  was calculated as

$$\chi = \frac{S_{\text{stress}} - S_{\text{iso}}}{S_{\text{iso}}} \quad [2]$$

where  $S_{\text{stress}}$  is the observed signal (e.g.,  $F_{\text{red}}$ ,  $F_{\text{green}}$ , or  $E_{\text{FRET}}$ ) following the osmotic challenge, and  $S_{\text{iso}}$  is the same signal before the osmotic challenge, as shown by the yellow background of the time trace in Fig. 2B.

Supporting data, further experimental procedures, and a detailed analysis and validation of the volume modulation model are provided in *SI Appendix*. The code for our model, including a Matlab GUI, is available for download at <https://www.github.com/shaharsu/KdSim>.

**ACKNOWLEDGMENTS.** We thank A. L. DeVries for use of his osmometer and E. L. Snapp for helpful discussions and the kind donation of the mEGFP plasmid. We acknowledge funding from National Science Foundation Grant MCB 14-13256 for development of the volume-jump microscopy and National Institutes of Health Grant GM093318-01-08 for in vitro association measurements.

- Schreiber G, Fersht AR (1996) Rapid, electrostatically assisted association of proteins. *Nat Struct Biol* 3:427–431.
- Caplow M, Fee L (2002) Dissociation of the tubulin dimer is extremely slow, thermodynamically very unfavorable, and reversible in the absence of an energy source. *Mol Biol Cell* 13:2120–2131.
- Phillip Y, Kiss V, Schreiber G (2012) Protein-binding dynamics imaged in a living cell. *Proc Natl Acad Sci USA* 109:1461–1466.
- König I, et al. (2015) Single-molecule spectroscopy of protein conformational dynamics in live eukaryotic cells. *Nat Methods* 12:773–779.
- McConkey EH (1982) Molecular evolution, intracellular organization, and the quinary structure of proteins. *Proc Natl Acad Sci USA* 79:3236–3240.
- Chien P, Gierasch LM (2014) Challenges and dreams: Physics of weak interactions essential to life. *Mol Biol Cell* 25:3474–3477.
- Cohen RD, Pielak GJ (2017) A cell is more than the sum of its (dilute) parts: A brief history of quinary structure. *Protein Sci* 26:403–413.
- Makowski L, et al. (2008) Molecular crowding inhibits intramolecular breathing motions in proteins. *J Mol Biol* 375:529–546.
- Rabouille C, Alberti S (2017) Cell adaptation upon stress: The emerging role of membrane-less compartments. *Curr Opin Cell Biol* 47:34–42.
- Srivastava DK, Bernhard SA (1986) Metabolite transfer via enzyme-enzyme complexes. *Science* 234:1081–1086.
- Hausmann CD, Ibbra M (2008) Aminoacyl-tRNA synthetase complexes: Molecular multitasking revealed. *FEMS Microbiol Rev* 32:705–721.
- Muschol M, Rosenberger F (1997) Liquid-liquid phase separation in supersaturated lysozyme solutions and associated precipitate formation/crystallization. *J Chem Phys* 107:1953.
- Hyman AA, Simons K (2012) Cell biology. Beyond oil and water—phase transitions in cells. *Science* 337:1047–1049.
- Wirth AJ, Gruebele M (2013) Quinary protein structure and the consequences of crowding in living cells: Leaving the test-tube behind. *BioEssays* 35:984–993.
- Smith AE, Zhou LZ, Gorensk AH, Sense M, Pielak GJ (2016) In-cell thermodynamics and a new role for protein surfaces. *Proc Natl Acad Sci USA* 113:1725–1730.
- Cohen RD, Pielak GJ (October 4, 2016) Electrostatic contributions to protein quinary structure. *J Am Chem Soc* 138:13139–13142.
- Riback JA, et al. (2017) Stress-triggered phase separation is an adaptive, evolutionarily tuned response. *Cell* 168:1028–1040.e19.
- Hyman AA, Weber CA, Jülicher F (2014) Liquid-liquid phase separation in biology. *Annu Rev Cell Dev Biol* 30:39–58.
- Hoffmann EK, Lambert IH, Pedersen SF (2009) Physiology of cell volume regulation in vertebrates. *Physiol Rev* 89:193–277.
- Zlotek-Zlotkiewicz E, Monnier S, Cappello G, Le Berre M, Piel M (2015) Optical volume and mass measurements show that mammalian cells swell during mitosis. *J Cell Biol* 211:765–774.
- Hecht VC, et al. (2016) Biophysical changes reduce energetic demand in growth factor-deprived lymphocytes. *J Cell Biol* 212:439–447.
- Heo J, Meng F, Hua SZ (2008) Contribution of aquaporins to cellular water transport observed by a microfluidic cell volume sensor. *Anal Chem* 80:6974–6980.
- Son S, et al. (2015) Resonant microchannel volume and mass measurements show that suspended cells swell during mitosis. *J Cell Biol* 211:757–763.
- Burg MB, Kwon ED, Kültz D (1997) Regulation of gene expression by hypertonicity. *Annu Rev Physiol* 59:437–455.
- Ben-Ari Y, et al. (2010) The life of an mRNA in space and time. *J Cell Sci* 123:1761–1774.
- Guo M, Gelman H, Gruebele M (2014) Coupled protein diffusion and folding in the cell. *PLoS One* 9:e113040.
- Minton AP (2006) How can biochemical reactions within cells differ from those in test tubes? *J Cell Sci* 119:2863–2869.
- Boersma AJ, Zuhorn IS, Poolman B (2015) A sensor for quantification of macromolecular crowding in living cells. *Nat Methods* 12:227–230.
- Kuznetsova IM, Turoverov KK, Uversky VN (2014) What macromolecular crowding can do to a protein. *Int J Mol Sci* 15:23090–23140.
- Wang Y, Sarkar M, Smith AE, Krois AS, Pielak GJ (2012) Macromolecular crowding and protein stability. *J Am Chem Soc* 134:16614–16618.
- Dhar A, et al. (2010) Structure, function, and folding of phosphoglycerate kinase are strongly perturbed by macromolecular crowding. *Proc Natl Acad Sci USA* 107:17586–17591.
- Burg MB (2002) Response of renal inner medullary epithelial cells to osmotic stress. *Comp Biochem Physiol A Mol Integr Physiol* 133:661–666.
- Hopewell B, Urban JPG (2003) Adaptation of articular chondrocytes to changes in osmolality. *Biorheology* 40:73–77.
- Brocker C, Thompson DC, Vasilou V (2012) The role of hyperosmotic stress in inflammation and disease. *Biomol Concepts* 3:345–364.
- Strange K (2004) Cellular volume homeostasis. *Adv Physiol Educ* 28:155–159.
- De Sancho D, Doshi U, Muñoz V (2009) Protein folding rates and stability: How much is there beyond size? *J Am Chem Soc* 131:2074–2075.
- van den Berg J, Boersma AJ, Poolman B (2017) Microorganisms maintain crowding homeostasis. *Nat Rev Microbiol* 15:309–318.
- Milo R (2013) What is the total number of protein molecules per cell volume? A call to rethink some published values. *BioEssays* 35:1050–1055.
- Lakowicz JR (2008) *Principles of fluorescence spectroscopy*, 3rd Ed (Springer, Berlin).
- Nunes P, et al. (2013) Hypertonic stress promotes autophagy and microtubule-dependent autophagosomal clusters. *Autophagy* 9:550–567.
- Rivas G, Minton AP (2016) Macromolecular crowding in vitro, in vivo, and in between. *Trends Biochem Sci* 41:970–981.
- Ohashi T, Galiacy SD, Briscoe G, Erickson HP (2007) An experimental study of GFP-based FRET, with application to intrinsically unstructured proteins. *Protein Sci* 16:1429–1438.
- Costantini LM, Fossati M, Francolini M, Snapp EL (2012) Assessing the tendency of fluorescent proteins to oligomerize under physiologic conditions. *Traffic* 13:643–649.
- Stepanenko OV, Verkhusha VV, Kuznetsova IM, Uversky VN, Turoverov KK (2008) Fluorescent proteins as biomarkers and biosensors: Throwing color lights on molecular and cellular processes. *Curr Protein Pept Sci* 9:338–369.
- Truong K, Ikura M (2001) The use of FRET imaging microscopy to detect protein-protein interactions and protein conformational changes in vivo. *Curr Opin Struct Biol* 11:573–578.
- Harris JI, Perham RN (1968) Glycerinaldehyde 3-phosphate dehydrogenase from pig muscle. *Nature* 219:1025–1028.
- Minton AP, Wilf J (1981) Effect of macromolecular crowding upon the structure and function of an enzyme: Glycerinaldehyde-3-phosphate dehydrogenase. *Biochemistry* 20:4821–4826.
- Watson HC, et al. (1982) Sequence and structure of yeast phosphoglycerate kinase. *EMBO J* 1:1635–1640.
- Ebbinghaus S, Dhar A, McDonald JD, Gruebele M (2010) Protein folding stability and dynamics imaged in a living cell. *Nat Methods* 7:319–323.
- Fokina KV, Dainyak MB, Nagradova NK, Muronetz VI (1997) A study on the complexes between human erythrocyte enzymes participating in the conversions of 1,3-diphosphoglycerate. *Arch Biochem Biophys* 345:185–192.
- Ashmarina LI, Muronetz VI, Nagradova NK (1985) Yeast glycerinaldehyde-3-phosphate dehydrogenase. Evidence that subunit cooperativity in catalysis can be controlled by the formation of a complex with phosphoglycerate kinase. *Eur J Biochem* 149:67–72.
- Tomokuni Y, et al. (2010) Loose interaction between glycerinaldehyde-3-phosphate dehydrogenase and phosphoglycerate kinase revealed by fluorescence resonance energy transfer-fluorescence lifetime imaging microscopy in living cells. *FEBS J* 277:1310–1318.
- Sirover MA (2011) On the functional diversity of glycerinaldehyde-3-phosphate dehydrogenase: Biochemical mechanisms and regulatory control. *Biochim Biophys Acta* 1810:741–751.
- Graciet E, Lebreton S, Camadro JM, Gontero B (2003) Characterization of native and recombinant A4 glycerinaldehyde 3-phosphate dehydrogenase. Kinetic evidence for conformation changes upon association with the small protein CP12. *Eur J Biochem* 270:129–136.
- Szabó J, et al. (2008) Communication between the nucleotide site and the main molecular hinge of 3-phosphoglycerate kinase. *Biochemistry* 47:6735–6744.
- Beck M, et al. (2011) The quantitative proteome of a human cell line. *Mol Syst Biol* 7:549.
- Arkin A, Ross J (1994) Computational functions in biochemical reaction networks. *Biophys J* 67:560–578.
- Munder MC, et al. (2016) A pH-driven transition of the cytoplasm from a fluid- to a solid-like state promotes entry into dormancy. *Elife* 5:1–30.
- Morris CE, Wang JA, Markin VS (2003) The invagination of excess surface area by shrinking neurons. *Biophys J* 85:223–235.